

Technical Note: Correlation of respiratory motion between external patient surface and internal anatomical landmarks

Hadi Fayad,^{a)} Tinsu Pan,^{b)} Jean François Clement,^{a)} Dimitris Visvikis^{a)}

5

^{a)} INSERM U650, LaTIM, CHU Morvan, Brest, F-29200 France

^{b)} Department of Imaging Physics, M.D. Anderson Cancer Center, Houston, Texas, USA

Purpose: Current respiratory motion monitoring devices used for motion synchronization in medical imaging and radiotherapy provide either 1D respiratory signals over a specific region or 3D information based on few external or internal markers. On the other hand, newer technology may offer the potential to monitor the entire patient external surface in real time. The main objective of this study was to assess the motion correlation between such an external patient surface and internal anatomical landmarks motion.

10

Methods: Four dimensional Computed Tomography (4D CT) volumes for ten patients were used in this study. Anatomical landmarks were manually selected in the thoracic region across the 4D CT datasets by two experts. The landmarks included normal structures as well as the tumour location. In addition, a distance map representing the entire external patient surface, which corresponds to surfaces acquired by a Time of Flight (ToF) camera or similar devices, was created by segmenting the skin of all 4D CT volumes using a thresholding algorithm. Finally, the correlation between the internal landmarks and

15

external surface motion was evaluated for different regions (placement and size) throughout a patient's surface. **Results:** Significant variability was observed in the motion of the different parts of the external patient surface. The larger motion magnitude was consistently measured in the central regions of the abdominal and the thoracic areas for the different patient datasets considered. The highest correlation

20

coefficients were observed between the motion of these external surface areas and internal landmarks such as the diaphragm and mediastinum structures as well as the tumour location landmarks (0.8 ± 0.18 and 0.72 ± 0.12 for the abdominal and the thoracic regions respectively). Worse correlation was observed

25

when one considered landmarks not significantly influenced by respiratory motion such as the apex and the sternum. **Discussion and conclusions:** There were large differences in the motion correlation observed considering different regions of interest placed over a patients' external surface and internal

30

anatomical landmarks. The positioning of current devices used for respiratory motion synchronization may reduce such correlation by averaging the motion over correlated and poorly correlated external

regions. The potential of capturing in real-time the motion of the complete external patient surface as well as choosing the area of the surface that correlates best with the internal motion should allow reducing such variability and associated errors in both respiratory motion synchronization and subsequent motion modeling processes.

Key words: respiratory motion, patient external surface, 4D CT.

I. INTRODUCTION

Respiratory motion reduces the qualitative and quantitative accuracy of multimodality imaging as well as the precision in the dose delivered to tumor and healthy tissues during radiation therapy (RT). To minimize the impact of respiratory induced organ and tumor motion different methods have been developed. The AAPM Task Group 76 report¹ lists five different approaches to deal with respiratory motion in treatment planning: (1) motion-encompassing methods²; (2) forced shallow breathing³; (3) breath hold⁴; (4) gating⁵; and (5) respiratory-synchronized radiotherapy offered currently by the CyberKnife system⁶ (Accuray Inc, Sunnyvale, US) or in the future through the use of Dynamic Multileaf collimators⁷.

The most advanced methods are based on modeling the respiratory motion and incorporating the information extracted from these models to improve dose calculation and delivery during RT. For example in the case of the CyberKnife SynchronyTM system a set of three optical fiducial markers are attached to a snugly fitting vest the patient wears during treatment, to provide a breathing signal. The only current recommendation for the placement of the external markers is either on the chest or the abdomen remaining visible by the optical tracking system used to monitor their position^{6,8}. In order to ensure continuous correspondence between the external and internal motion^{6,8}, small gold markers are also implanted prior to treatment in the vicinity of the target organ or lesion, allowing a model to be defined between the motion of the external and internal markers. This model is updated based on frequent x-ray snapshots of the position of both marker sets simultaneously⁸. A technology that can potentially eliminate the need for an internal – external motion model involves the use of the Calypso system (Calypso Medical Technologies, Seattle, US) which uses implanted transponders with an associated wireless tracking with a frequency of up to 10Hz^{9,10}. However, the issue remains the use of implanted markers which involves an invasive procedure. A potential alternative to the use of implanted markers will be modeling the internal structure motion using respiratory phase and amplitude information in association with displacement fields derived from 4D CT acquisitions using deformable registration^{11,12}. However, any such model depends on the accuracy of the phase and amplitude motion information which is currently derived by external markers.

In the literature, several studies have concentrated in the past on investigating the external-internal motion correlation. Mageras et al.¹³ and Vedam et al.¹⁴ have shown a strong correlation between external markers and the diaphragm but their study did not include tumor motion. Gierga et al.¹⁵ used fluoroscopy to gather tumor respiratory motion data, recording this information using standard video recorder interfaced with the fluoroscopy monitor. Results of this study indicated that abdominal tumor motion correlates well with the external markers placed on the patient's abdominal skin. A good correlation was found between the motion frequency of the external and internal markers. However, in the same study, a substantial variability was observed in the tumor location considering a given position in the respiratory cycle. This variability was dependent on the external marker location, subsequently affecting the tumor to external marker motion ratio. Finally, this study did not include an assessment of the reproducibility of the observed correlation, neither a study of the potential correlation of phase between internal and external motion.

Tsunashima et al.¹⁶ studied the correlation between the 1D respiratory waveform measured by an external sensor and the 3D tumor motion. Different tumor types were considered which included lung, liver and esophagus. The correlation between the respiratory waveform and tumor motion showed the difficulty to obtain information from the respiratory waveform inhale phase because of the short inspiration period. In addition, a phase shift was observed between the 3D tumor motion and the respiratory signal. This shift was variable and in the range of 0.0 to 0.3s regardless of the organ being measured, which means that the respiratory waveform may not always express the 3D tumor motion with fidelity. Within the same context, Beddar et al.¹⁷ studied the correlation between the respiratory signal and liver tumors. They also noted that, in some cases, internal anatomical landmarks do not move in synchrony with the 1D respiratory signal also implying that such an 1D signal may not adequately describe tumor respiratory motion.

All these studies indicate that external 1D surrogate measures of respiratory motion may correlate with tumor motion but with non-negligible amplitude and phase differences. These two parameters obtained through regular monitoring need to be taken into consideration in any respiratory motion model in order to ensure that external surrogate measures predict well internal tumor motion. On the other hand, the existing studies also suggest that the position of the external surrogates and the acquisition protocol used can influence the observed internal-external motion correlation in an arbitrary fashion. In order to overcome the observed variability associated with the location of the external markers¹ we have previously proposed the use of patient surface monitoring using a novel external detection system¹⁸, without the need for invasive internal or external markers. This system consists of a Time of Flight (ToF) camera¹⁹ which actively illuminates the patient with an incoherent light signal and captures the reflected light allowing 3D distance maps of the patient surface to be acquired with rates of up to 30Hz. Alternative techniques that may also facilitate a complete 3D patient surface observation include the use of speckle projection as in the case of the

VisionRT™ system^{20,21} (Vision RT Ltd, London, UK). As our previous study has demonstrated¹⁸ considering such information allows an improved accuracy in modeling patient specific respiratory motion compared to using 1D
95 respiratory signal information. However, in order to optimize the utilization of the information provided by the patient dynamic external surface maps there is first a need to understand the correlation between the motion of the external patient surface, to be used as a surrogate measure of respiratory motion, and the internal organ/structures motion.

Therefore the objective of this work was to study the correlation between a patient external surface and internal structures' displacement due to respiratory motion. This correlation was studied using the segmented external patient
100 surfaces from 4D CT patient images and internal landmark identification by experts.

II. MATERIALS AND METHODS

A. CT datasets

The clinical datasets used in this study were acquired on a GE Lightspeed 8-slice CT with cine CT scan capability²².
105 Each cine CT scan covered 2cm (8*2.5mm) with 19 to 23 images acquired per slice location. A 0.5 s gantry rotation was used to ensure a high temporal resolution. The interval between each cine image was 0.45 sec. The total axial length covered in the cine CT acquisition for each patient was 28cm. The real-time position management (RPM, Varian Medical Systems) system was used to obtain the patient's respiration signal²³. No specific indication on how to breathe was given to the patients, but they were asked to breathe normally and regularly.

110 The acquired 4D CT images were sorted using an improved phase binning approach by rejecting parts of the respiratory cycle and corresponding CT images associated with irregular respiration as described by Pan et al²². Binned 4D CT series were composed of ten phases (0%, 10%...up to 90% of a mean respiratory cycle). The software used searches for each slice location the CT image whose phase is closest to the one of the ten phases. Each binned thoracic CT volume had 512*512*112 voxels, with dimensions 0.97*0.97*2.5mm³ corresponding to the x, y and z directions
115 respectively). 4D CT datasets from 10 patients were used in this study. For all of these patient datasets no motion or streak artifacts were visually detectable by an experienced radiologist in any of the ten binned CT volumes.

B. Anatomical Landmark Motion Measurements

Two clinical oncologists were asked to select some easily identified anatomical landmarks in all of the 4D CT
120 images for the 10 patient datasets. These points were placed in regions with high and low expected displacements during respiration^{24,25}. As a result, 13 anatomical landmarks, covering all the regions of the thorax were used in this study. These included the right and left apex, the aortic cross, the sternum, the carina, the right and left nipples, the right and left diaphragm "highest" position and the upper, low, left and right boundaries of the tumor (see Figure 1).

The motion of these points was subsequently extracted by calculating the 3D distance between these landmarks considering for each patient all respiratory synchronized 4D CT image series. An example of this distance in the case of the right diaphragm higher position landmark is shown in figure 2 and is given by the following equation:

$$D(l) = \sqrt{(q_x^k - r_x^k)^2 + (q_y^k - r_y^k)^2 + (q_z^k - r_z^k)^2} \quad (1)$$

where, q_x^k , q_y^k and q_z^k are respectively the x, y and z coordinates of the k-th landmark in the reference CT corresponding to the end expiration position (x, y, and z represent the components in the three dimensions) and r_x^k , r_y^k and r_z^k are respectively the x, y and z coordinates of the k-th landmark in the other 4D CT frames corresponding to the remaining nine phases. The calculated distance was recorded in mm.

The two clinical oncologists were asked to repeat once the same task of identifying the anatomical landmarks on the 4D CT images of all 10 patients considered in the study. The repeatability of the anatomical landmarks identification from the two experts were compared separately (intra-observer variability) and to each other (inter-observer variability)²⁶.

C. External Surface Motion Measurements

4D CT volumes were segmented using a threshold based segmentation algorithm²⁷ and patient surfaces were extracted. Each extracted surface corresponds to a binary 3D volume, with the voxels constituting the patient's surface set to 1 and all other voxels set to 0. In addition, a distance map representing the distance of the patient skin from a given plane was calculated. This latter map corresponds to the distance map that can be acquired by a ToF camera¹⁹, capable of yielding 3D surface maps (acquisition rate >30Hz) in which each point corresponds to the measured Euclidean distance between the camera and the object.

A number of regions of interest (ROI) were subsequently placed on the calculated distance map in order to simulate the specific location of external markers. Given the external surface pixel's dimension of $0.97 \times 2.5 \text{ mm}^2$ (corresponding to the x and z directions of a CT volume respectively), circular regions of 15×6 pixels (Figure 3(a)) and square zones of 25×10 pixels (Figure 4(a)) were used. In addition, rectangular regions of 300×6 pixels (Figure 5(a)) were used to simulate regions corresponding to the placement of a pressure belt frequently used for the registration of a patient's 1D respiratory signal²⁸.

D. Internal-External Motion Correlation

The correlation coefficient (CC) measures a linear affine relationship between the motion measured on the internal landmarks (I) considered and the external (E) regions of interest placed on the extracted distance maps (CC of 1 indicates a perfect external-internal motion correlation). The CC is defined as follow:

$$155 \quad CC(I,E) = \frac{(i - m_I)(e - m_E)}{\sqrt{\sigma_I} \sqrt{\sigma_E}} \quad (2)$$

where, i and e are internal and external displacements respectively, m_I and m_E are the mean of an internal point and external ROI motion, σ_I and σ_E are the standard deviations of the internal and external motion respectively. For each anatomical landmark the mean motion calculated by the two experts was used.

160 III. RESULTS

The repeatability results in identifying the internal anatomical landmarks by the two clinical oncologists revealed an intra-operator variability of 1.7 ± 0.7 mm and 1.9 ± 0.6 mm for the first and the second expert respectively. In terms of inter-operator reproducibility a difference of 1.1 ± 0.4 mm and 1.7 ± 0.6 mm were measured considering the two repeated anatomical landmark identifications from the two oncologists. Therefore both intra- and inter-operator reproducibility results showed average differences smaller than the largest distance between two neighboring voxels (2.5mm). Variable motion amplitude was measured for the different internal anatomical landmarks considered. For example, the mean motion amplitude and corresponding standard deviation measured on the 10 patients included in this study was 18.1 ± 6.6 mm, 3.0 ± 1.2 mm and 12.3 ± 8.1 mm for the left diaphragm, the apex and the lower tumour landmark (see figure 1) respectively.

170 Considering the correlation between the external regions' motion and that of the internal anatomical landmarks, figure 3(a) shows the position of the six small ROIs placed on the external patient surface (see also section II.C). Considering all patients the mean and standard deviation of the correlation between all 13 internal landmarks and the 6 external ROIs of figure 3(a) is shown in figure 3(b). A more detailed correlation between each of these external points and individual internal landmarks is shown in figures 3(c) and 3(d) for the normal anatomical landmarks and those concerning the tumor location respectively. As shown in this figure, internal anatomical landmarks such as the aortic cross, the carina, the diaphragm and those associated with the tumor location show higher correlation with the motion of the external ROIs than the apex or the sternum which exhibit the smaller motion amplitude of the different internal landmarks considered. In addition, a much lower correlation is obtained when one is considering the more peripherally placed external regions (i.e. ROIs 5 and 6 in figure 3(a)).

180 Figure 4(a) shows the 13 horizontal rectangular external regions considered (see also section II.C). For all patients considered, the mean and standard deviation of the motion correlation between these external rectangular regions and

all of the internal landmarks are shown in figure 4(b). A higher correlation in the measured motion is shown for the ROIs placed over the abdominal and thoracic areas rather than the regions located in-between. The amplitude of motion in the abdominal ROIs (regions 12 and 13, see figure 4(a)) was on average a factor of two higher than the thoracic ROIs (regions 1 to 4, see figure 4(a)), while there was very little motion seen in the in-between ROIs ($0.2\pm 0.8\text{mm}$). On the other hand, no phase shifts were observed between the motion of the centrally arranged abdominal and thoracic regions. As noticed before, the correlation between external ROIs and the aortic cross, the carina, the diaphragm and the tumor location is clearly better than the correlation with the motion of the apex or the sternum (figures 4(c) and 4(d)).

In addition as shown in figure 5(a), small square vertical regions were placed over the abdominal area, which has consistently across the different patients considered demonstrated the largest amplitude motion of the external patient surface. The objective was to demonstrate which specific part over that region correlates the most with the internal landmarks' motion. The results show (see figure 5(b)) that the central region surrounding the umbilicus correlates the most with the internal landmark motion. The motion measured in this central abdominal region (3 to 8, see figure 5(a)) was larger by a factor of three relative to the side regions (1 to 2 and 9-11, see figure 5(a)). The worse correlation measured for these peripherally placed regions was associated with a phase shift in the measured motion relative to the more centrally located ROIs or the internal anatomical landmark motion. As figure 5(c) demonstrates this correlation is stronger when the less correlated internal landmarks identified before (apex and sternum) are excluded. The assumption behind the removal of these internal landmarks from the correlation analysis is that regions like the apex and the sternum are, as observed, influenced very little by respiratory motion.

Finally, figure 6 describes the variation observed in the external-internal landmarks motion correlation amongst four different patients included in the study. Figure 6(a) shows the patient respiratory traces demonstrating the variability in both the rate and amplitude of the motion. Despite this variability there is a high correlation between the motion associated with the external surface regions in the abdominal area and the internal anatomical landmarks. This is true for the landmarks associated with the normal structures (diaphragm, mediastinum structures) as well as those describing the tumour motion as shown in figures 6(b) and 6(c) respectively.

IV. DISCUSSION AND CONCLUSIONS

Respiratory motion synchronization in medical imaging and external beam radiotherapy is currently based on the use of devices which are providing a respiratory signal trace used for synchronization purposes. This process is based on the assumption that a good correlation exists between the respiration induced motion of external surrogate measures and internal structures. Within this context different studies have already been performed demonstrating variable correlation between external markers and internal anatomical structures such as the diaphragm or tumour motion. In all

of these studies external markers were placed on specific positions of the patient's skin. On the other hand, the correlation with the respiration induced motion of internal structures has been studied considering either normal anatomical landmarks or the tumour motion but rarely both.

Current technology used routinely for respiratory motion synchronization provides only an 1D respiratory signal over a limited area of the external patient's surface, such as the use of a pressure-sensitive belt over the chest or abdomen²⁸, and the use of passive infrared reflective markers placed on a patient's torso²³. Alternative approaches based on the use of implanted markers have been also proposed, such as the use of gold seeds for real time tumour tracking^{1,29,30} or in the context of providing a real-time update for an internal structure – external markers motion model in the case of the CyberKnife SynchronyTM system⁶, as well as the use of electromagnetic transponders whose location is monitored using the Calypso system^{9,10}.

On the other hand, technologies such as the VisionRTTM system^{20,21} or a ToF camera^{9,10} allow real-time monitoring of a patient's surface. Such an approach presents certain advantages over other devices, noticeably a **marker-less** fashion to monitor respiratory motion since no contact with the patient is needed as is the case with external (fiducial, optical, magnetic) or implanted markers, and pressure belts. **The only prerequisite of these devices is that the patient should wear a snugly fitting vest during surface acquisition or alternatively being shirtless.** In addition, a ToF camera allows monitoring the motion of the complete patient surface in a high frequency rate making available substantially more information for respiratory synchronised acquisitions or therapy compared to location specific 1D respiratory signals. Additional advantages of the ToF camera technology include its small size and the fact that in principle no prior calibration is required. In this study, equivalent information to that provided by systems capturing the motion of a patient's external surface was derived using 4D CT acquisitions of ten patients. The objective was to investigate the level of correlation between the motion of different regions of the external patient's surface and multiple internal anatomical landmarks corresponding to normal structures as well as the tumour.

The results of this study indicate that there exists a correlation between the motion induced by respiration in parts of the external patient surface and internal anatomical landmarks. The motion of chest and abdominal regions seems to correlate the best with different internal anatomical landmarks including those describing the tumour motion. This observed correlation seems to be consistent despite the variability in the motion amplitude observed for the 10 patients considered in this study. No phase shifts were observed between the motion of the chest and abdominal surface regions. Internal normal anatomical landmarks demonstrating high correlation in terms of respiration induced motion with regions of the external patient's surface include the diaphragm, and mediastinum structures such as the aortic cross and the carina. On the other hand, poor correlation associated with motion phase shifts was measured between these same internal anatomical landmarks and peripherally located surface regions in the abdomen and chest. Finally, anatomical

landmarks such as the apex and the sternum, showing the smallest amplitude respiratory induced motion, were poorly
245 correlated with the external patient's surface motion.

The difference in the motion correlation observed considering different regions of interest placed over a patients' external surface hint to potential issues associated with the use and positioning of current devices for respiratory synchronization. More specifically such 1D respiratory traces are either derived from regions over which a variable correlation exists between external and internal motion (for example areas covered by pressure-sensitive belts) or
250 through the specific placement of external markers (for example in the case of infrared reflective markers). Existing recommendations considering the positioning of such markers with the Varian RPM™ system suggest their placement typically midway between the xyphoid process and the umbilicus¹, chosen in order to maximize the AP respiratory induced motion. In our study, this position was amongst the surface regions representing a good correlation between external and internal structure motion including that of the tumour. Another example is the proposed placement on the
255 chest or abdomen of the three external optical markers used with the CyberKnife Synchrony™ system. Our study demonstrates that the level of the placement of such markers could have a substantial impact since there is little motion and hence a worse correlation between internal landmarks and external markers in the zone located between the chest and the abdominal region. In addition, within these regions (chest and abdomen) keeping the placement of the markers centrally rather than peripherally will also help in increasing the expected internal landmark and external fiducials
260 motion correlation.

Clearly the ability to measure in real-time the motion of the complete external patient surface will allow reducing such variability and associated errors. This may be achieved by considering in the subsequent motion synchronization and modeling processes only those regions of interest demonstrating the best correlation with the internal structures' respiratory motion induced displacements. Finally, ensuring a good correlation between internal and external motion
265 could help in reducing the need for implanted devices which involve invasive procedures. However, given that our study was based on 4D CT acquisitions created using an average, although patient specific, respiratory motion, it will be always necessary to use an adaptative internal-external correlation which is able to dynamically capture any correlation changes in order to accurately predict the internal target position.

A limitation of the current study is that it has not considered the errors in terms of accuracy with which a device,
270 such a ToF camera, can determine in a real-time fashion the motion amplitude due to respiration throughout a patient surface. Preliminary studies have suggested that this accuracy may be <2mm, with a minimum variability throughout the camera's field of view³¹. These experimental estimations have to be clearly verified on datasets comprising simultaneous patient 4D CT acquisitions and external surface measurements using such devices.

275

V. REFERENCES

- ¹ Keall P.J., Mageras G.S., Balter J.M., Emery J.S., Forster K.M., Jiang S.B., Kapatoes J.M., Low D.A., Murphy M.J., Murray B.R., Ramsey C.R., Van Herk M.B., Vedam S.S., Wong J.W. and E. Yorke "The management of respiratory motion in radiation oncology report of AAPM Task Group 76" AAPM Report 91, Med. Phys. 33 3874-3900 (2006).
- 280 ² Van Herk M. "Errors and margins in radiotherapy" Seminars in Radiation Oncology 14 52-64 (2004).
- ³ McGarry R.C., Papiez L., Williams M. and R.D. Timmerman "Stereotactic body radiation therapy of early-stage non-small-cell lung carcinoma: Phase 1 study" Int. J. Radiat. Oncol. Biol. Phys. 63 1010-1015 (2005).
- ⁴ Nakamura K., Shioyama Y., Nomoto S., Ohga S., Toba T., Yoshitake T., Anai S., Terashima H. and H. Honda "Reproducibility of the abdominal and chest wall position by voluntary breath-hold technique using a laser-based monitoring and visual feedback system" Int. J. Radiat. Oncol. Biol. Phys. 68 267-272 (2007).
- 285 ⁵ Ohara K., Okumura T. and M. Akisada "Irradiation synchronized with respiration gate" Int. J. Radiat. Oncol. Biol. Phys 17 853-857 (1989).
- ⁶ Schweikard A., Glosser G., Bodduluri M., Murphy M.J. and J.R. Adler "Robotic motion compensation for respiratory movement during radiosurgery" Computer Aided Surgery 5 263-277 (2000).
- 290 ⁷ Keall P.J., Kini V.R., Vedam S.S. and R. Mohan "Motion adaptive x-ray therapy: a feasibility study" Phys. Med. Biol. 46 1-10 (2001).
- ⁸ Schweikard A, Shiomi H and Adler J "Respiration tracking in radiosurgery" Med. Phys. 31, 2738-2741 (2006).
- ⁹ Kupelian P, Willoughby T, Mahadevan A, Djemil T, Weinstein G, Jani S, Enke C, Solberg T, Flores N, Liu D, Beyer D, Levine L "Multi-institutional clinical experience with the Calypso System in localization and continuous, real-time monitoring of the prostate gland during external radiotherapy" Int J Radiat Oncol Biol Phys. 2007; 67(4):1088-1098.
- 295 ¹⁰ Santanam L, Malinowski K, Hubenschmidt J, Dimmer S, Mayse M, Bradley J, Chaudhari A, Lechleiter K, Esthappen J, Mutic S, Low D, and Parikh P. "Fiducial-Based Translational Localization Accuracy of Electromagnetic Tracking System and on-Board Kilovoltage Imaging System" Int J Radiat Oncol Biol Phys. 2008, 70(3): 892-899.
- ¹¹ McClelland J R, Blackall J M, Tarte S, Chandler A C, Hughes S, Ahmad S, Landau D B and Hawkes D J, 2006, A continuous 4D motion model from multiple respiratory cycles for use in lung radiotherapy Med. Phys., vol. 33, pp. 3348–3358, 2006.
- 300 ¹² Fayad H, Pan T, Roux C, Cheze Le Rest C, Pradier O and Visvikis D, 2009, A 2D-Spline Patient Specific Model for Use in radiation therapy IEEE ISBI conference proceedings, 1319 – 1322.
- ¹³ Mageras, G. S.; Pevsner, A.; Yorke, E et al. 2004 Measurement of lung tumor motion using respiration-correlated CT Int. J. Radiat. Oncol., Biol., Phys., 60, 933-941.
- 305 ¹⁴ Vedam, S.; Kini, V.; Keall, P. et al., 2003, Quantifying the predictability of diaphragm motion during respiration with a noninvasive external marker Med Phys, 30, 505–513.
- ¹⁵ Gierga, D.; Brewer, J.; Sharp, G. et al., 2005, The correlation between external and internal markers for abdominal tumors: implications for respiratory gating Int. J. Radiat. Oncol. Biol. Phys., 61(5), 1551-1558.
- ¹⁶ Tsunashima, Y.; Sakae, T.; Shioyama, Y. et al., 2004, Correlation between the respiratory waveform measured using A respiratory sensor and 3D tumor motion in gated radiotherapy Int. J. Radiat. Oncol. Biol. Phys., 60(3), 951-958.
- 310

17 Beddar, A.; Kainz, K.; Briere, T. M. et al., 2007, Correlation between internal fiducial tumor motion and external marker motion for liver tumors imaged with 4D-CT *Int. J. Radiat. Oncol. Biol. Phys.*, 67(2), 630-638.

18 Fayad H, Pan T, Roux C, Cheze-Le Rest C, Pradier O, Clement JF, Visvikis D, 2009, A Patient Specific Model Based On 4D CT Data and a Time of Flight Camera (ToF). *IEEE Nuclear Science Symposium and Medical Imaging Conference proceedings*, 2594-315 2598.

19 Schaller C, Penne J, Hornegger J 2008 Time-of-Flight Sensor for Respiratory Motion Gating. *Med Phys*; 35(7) : 3090-3093.

20 Christoph Bert, Katherine G. Metheany, Karen Doppke, George T. Y. Chen. A phantom evaluation of a stereo-vision surface imaging system for radiotherapy patient setup. *Med. Phys.* 32(9), 2753-2762, 2005.

21 P.J. Schoffel, W. Harms, G. Sroka-Perez, W. Schlegel and C.P. Karger. Accuracy of a commercial optical 3D surface imaging system for realignment of patients for radiotherapy of the thorax. *Physics in Medicine and Biology*; 52: 3949-3963; 2007. 320

22 Pan T, Sun X, and Luo D 2007 Improvement of the cine- CT based 4D-CT imaging *Med. Phys.*, vol. 34(11), pp.4499–4503.

23 SA Nehmeh, YE Erdi, and CC Ling, KE Rosenzweig, OD Squire, LE Braban, E Ford, K Sidhu, GS Mageras, SM Larson, JL Humm 2002 Effect of respiratory gating on reducing lung motion artifacts in PET imaging of lung cancer *Med. Phys.*, vol. 29(3), pp.366–371.

24 Giraud P, Reboul F, Clippe S, Garcia R, Carrie C, Campana F, Dubray B, Rosenwald J C, Cosset J M 2003 Respiration-gated radiotherapy: current techniques and potential benefits *Cancer Radiothérapie* 2003;7 Suppl 1:15s-25s. 325

25 Ionascu D, Jiang SB, Nishioka S, Shirato H, Berbeco RI. 2007 Internal-external correlation investigations of respiratory induced motion of lung tumors. *Med Phys.*; 34(10):3893-903.

26 Sarrut D, Boldea V, Miguet S and Ginestet C 2006 Simulation of 4D CT images from deformable registration between inhale and exhale breath-hold CT scans. *Medical Physics*, 33(3):605-617.

27 X. Zhou, T. Hara, H. Fujita, et al., 2004, Automated Segmentations of Skin, Soft-tissue and Skeleton from Torso CT images, *Proc. of SPIE-Medical Imaging*, vol. 5370, pp.1634-1639. 330

28 Kanoulas E, Aslam JA, Sharp GC, Berbeco RI, Nishioka S, Shirato H, and Jiang SB., 2007, Derivation of the tumor position from respiratory surrogates with periodical updating of internal/external correlation. *Phys Med Biol*, 52(17): 5443-5456.

29 K. Kitamura et al. "Registration accuracy and possible migration of internal fiducial gold marker implanted in prostate and liver treated with real-time tumor-tracking radiation therapy RTRT" 2002 *Radiother. Oncol.* 623, 275–281. 335

30 Shirato H et al. Physical aspects of a real-time tumor-tracking system for gated radiotherapy. *Int J Radiat Oncol Biol Phys.* 2000 Nov 1;48(4):1187-95.

31 JF Clement, H Fayad, M Lamard, C Cheze Le Rest, O Pradier, D Visvikis, 2009, Time of flight camera (ToF) for contact-less and marker-less 3D respiratory motion detection *J Nuc Med* 50, S2, 1541. 340

340

345

350

FIGURES CAPTION

355 **Figure 1:** Thirteen anatomical internal landmarks identified by radiation oncologists covering both normal and tumour structures.

Figure 2: Distance between the position of one of the considered anatomical landmarks (higher right diaphragm position) throughout the respiratory cycle as identified in the 4D CT image series.

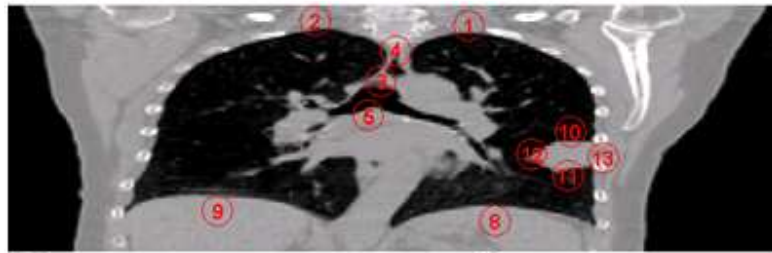
360 **Figure 3:** Analysis of the correlation between (a) six small regions of interest placed on the external surface (3 pixels diameter) and the internal landmarks (L1-L13) shown in figure 1. (b) Mean and standard deviation (error bars) of the measured motion correlation. Correlation between the motion of each external circular ROI considered with (c) the normal structure landmarks and (d) tumor landmarks motion.

365 **Figure 4:** Analysis of the correlation between (a) 14 rectangular regions covering the majority of the external surface and the internal landmarks (L1-L13) shown in figure 1. (b) Mean and standard deviation (error bars) of the measured motion correlation. Correlation between the motion of each external rectangular ROI considered with (c) the normal structure landmarks and (d) tumor landmarks motion.

370 **Figure 5:** Analysis of the correlation between (a) 11 square ROIs covering the abdominal region of the external patient surface and the internal landmarks (L1-L13) shown in figure 1. Mean and standard deviation (error bars) of the measured motion correlation (b) considering all of the internal anatomical landmarks and (c) after removal of the anatomical landmarks demonstrating very small respiratory motion (apex, sternum).

375 **Figure 6:** Patient specific measurements (a) 1D respiratory traces used in the synchronization process of the 4D CT acquisitions. (b) Correlation between different external abdominal ROIs (shown in figure 5(a)) and internal anatomical landmarks corresponding to normal structures (c) Correlation between different external abdominal ROIs (shown in figure 5(a)) and internal tumour landmarks.

380



- ① Right Apex
- ② Left Apex
- ③ Aortic Cross
- ④ Sternum
- ⑤ Carina
- ⑥ Left Nipple (can be determined on an another slice)
- ⑦ Right Nipple (can be determined on an another slice)
- ⑧ Right diaphragm highest position
- ⑨ Left diaphragm highest position
- ⑩ Tumor upper pole
- ⑪ Tumor down pole
- ⑫ Tumor left pole
- ⑬ Tumor right pole

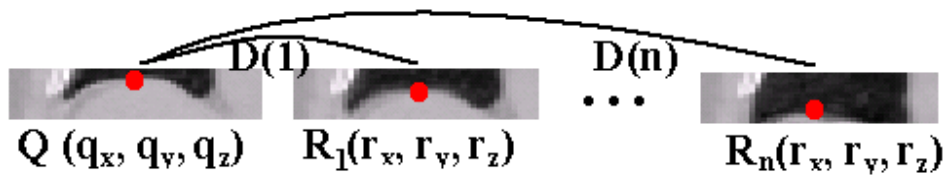
Figure 1.

385

390

395

400



405

Figure 2.

410

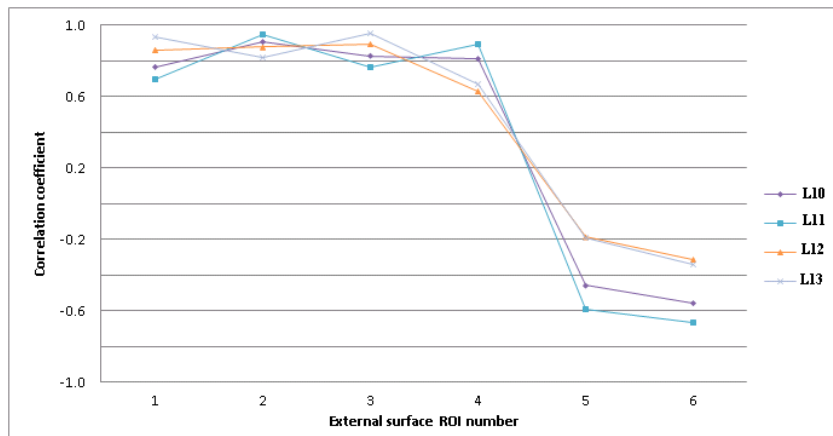
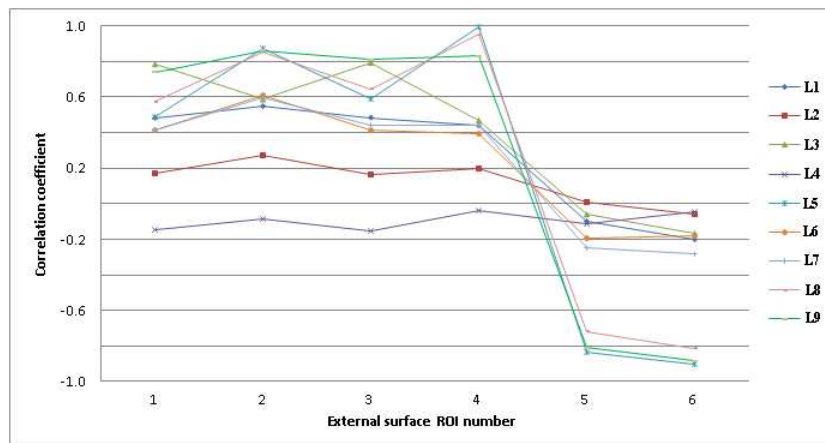
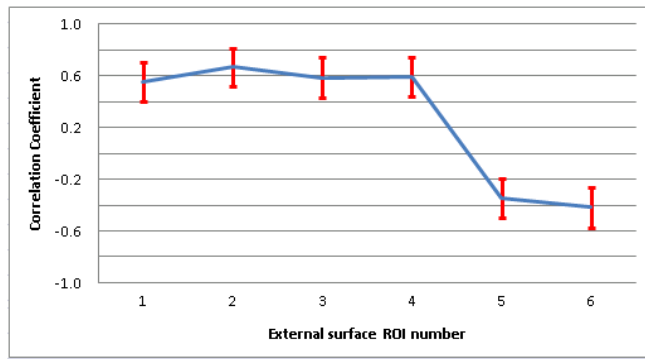
415

420

425

430

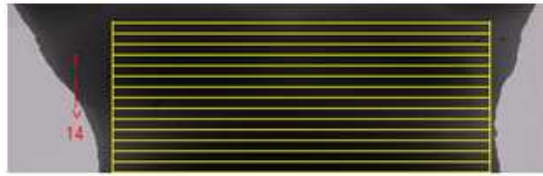
435



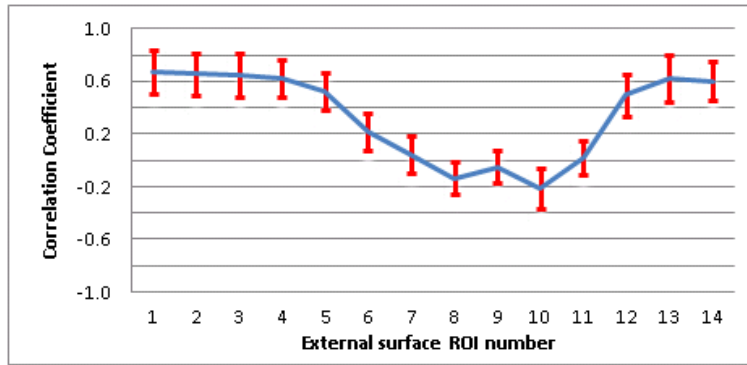
440

445

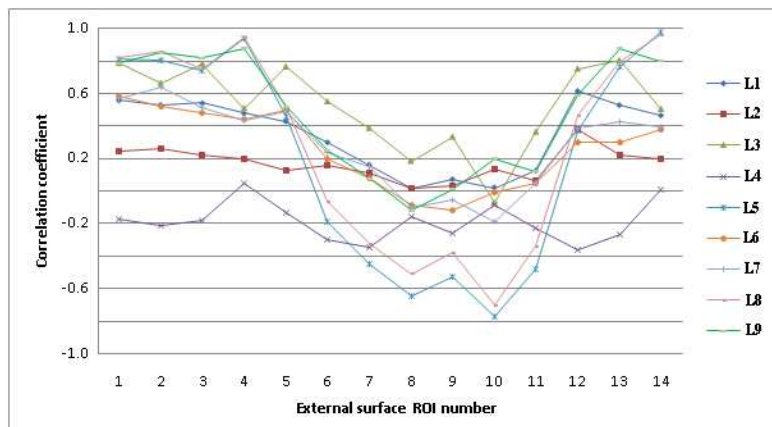
(d)
Figure 3.



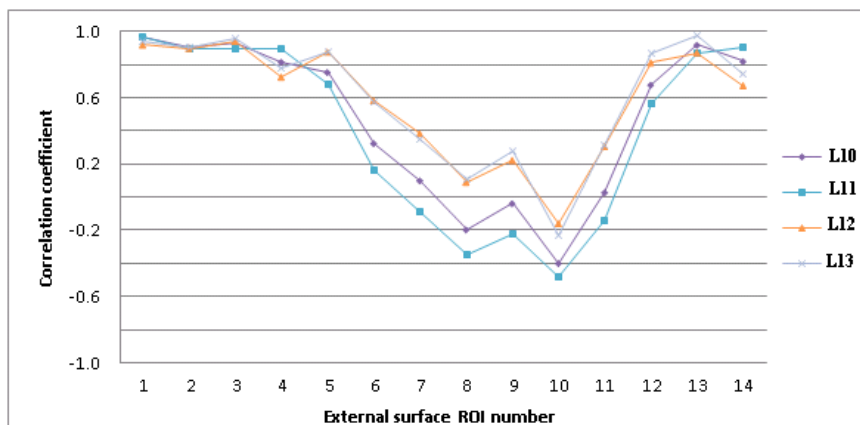
(a)



(b)



(c)



(d)

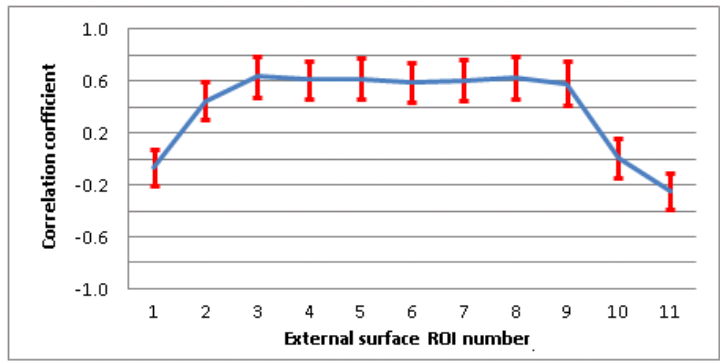
450

455

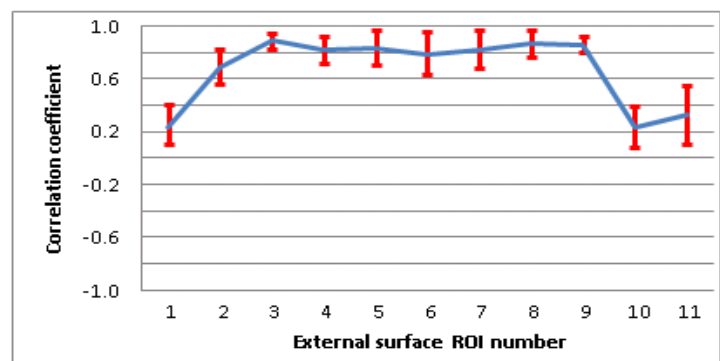
Figure 4.



(a)



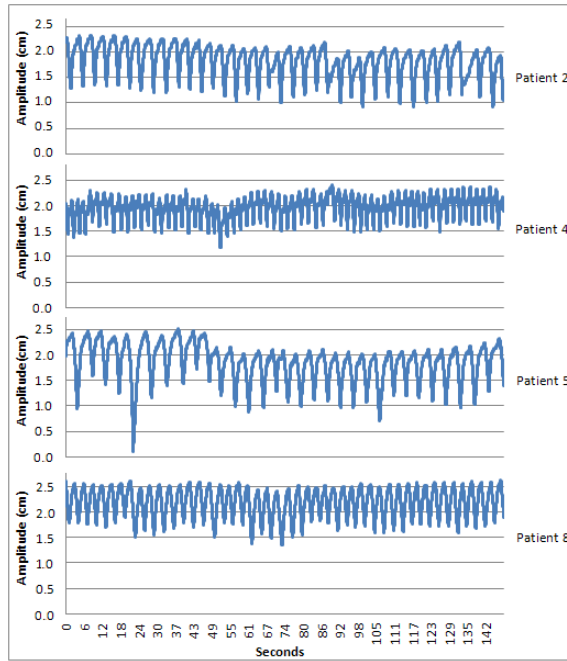
(b)



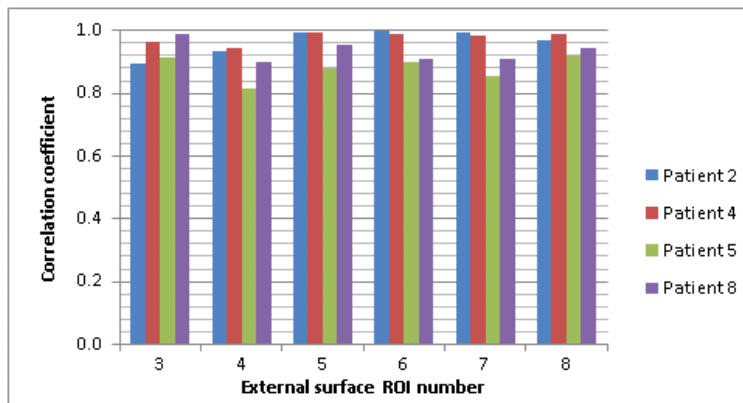
(c)

Figure 5.

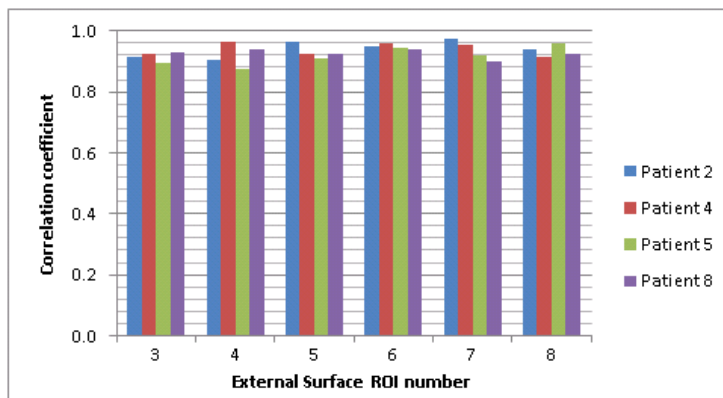
465



(a)



(b)



(c)

Figure 6.